# Discontinuity-Induced Bifurcations in Systems With Hysteretic Force Interactions

**Harry Dankowicz**[1]
Department of Mechanical Science and Engineering,
University of Illinois at Urbana-Champaign,
Urbana, IL 61801
e-mail: danko@illinois.edu

**Mark R. Paul**
Department of Mechanical Engineering,
Virginia Polytechnic Institute and State University,
Blacksburg, VA 24061
e-mail: mrp@vt.edu

*This paper presents the application of the discontinuity-mapping technique to the analysis of discontinuity-induced bifurcations of periodic trajectories in an example hybrid dynamical system in which changes in the vector field associated with the crossing of a discontinuity-surface depend on the direction of crossing. The analysis is motivated by a hysteretic model of the capillary force interactions between an atomic-force-microscope cantilever probe tip and a nanoscale sample surface in the presence of a thin liquid film on the tip and the surface and operating in intermittent-contact mode. The analysis predicts the sudden termination of branches of periodic system responses at parameter values corresponding to grazing contact with the onset of the hysteretic force interactions. It further establishes the increase beyond all bounds of the magnitude of one of the eigenvalues of the linearization of a suitably defined Poincaré mapping, indicating the destabilizing influence of near-grazing contact.* [DOI: 10.1115/1.3192131]

## 1 Introduction

Nonlinearities are an essential feature of the interactions between mechanical elements at the nanoscale. Attempts to ignore their influence and to establish nanoscale devices based solely on linear characteristics are bound to fall short of harvesting the full potential of the nanoscale regime. But with this recognition does not automatically come enlightenment as nonlinear phenomena are inherently more complicated to characterize, model, analyze, and control. This affords an opportunity for nonlinear analysis, in general, and nonlinear dynamical systems methods, in particular, to make substantial contributions to the successful deployment of nanotechnology.

A strong source of nonlinearity in dynamical systems is the presence of system discontinuities across which sudden changes occur in the force description (e.g., Fillippov systems [1]) or at which sudden changes occur in the system state (e.g., systems with impacts [2]). In addition to the bifurcations in system behavior characteristic of otherwise smooth systems, systems with discontinuities may exhibit *discontinuity-induced* bifurcations that are directly associated with singular interactions of steady-state system trajectories with the discontinuities (see Ref. [3]). These include *border-collision* bifurcations in which a fixed point of an associated Poincaré map crosses a discontinuity separating two distinct vector fields and *grazing* bifurcations in impact oscillators associated with the onset of low-relative-velocity contact between parts of a mechanism along a nonimpacting periodic oscillation.

The *discontinuity-mapping* technique originating in the work of Nordmark and collaborators (e.g., Refs. [1,2,4,5]) provides a local description of the system dynamics and the effects of the discontinuity in the vicinity of a point of tangential contact of system trajectories with the discontinuity surface. The present paper presents the first application of this technique to the near-grazing bifurcation analysis of a periodic trajectory in a hybrid dynamical system in which the change in the vector field associated with crossing a discontinuity surface depends on the direction of crossing.

[1]Corresponding author.

Contributed by the Design Engineering Division of ASME for publication in the JOURNAL OF COMPUTATIONAL AND NONLINEAR DYNAMICS. Manuscript received July 23, 2008; final manuscript received March 31, 2009; published online August 25, 2009. Review conducted by Lawrie Virgin. Paper presented at the Eighth Biennial ASME Conference on Engineering Systems Design and Analysis (ESDA2008), Haifa, Israel, July 7–9, 2008.

## 2 Degeneracies in Models of AFM Dynamics

The interactions in intermittent-contact mode between an atomic-force-microscope (AFM) cantilever probe and a sample surface are characterized by ranges in the tip-sample separation over which rapid changes occur in the nature and magnitude of the interaction forces. Where long-range attractive van der Waals-type forces dominate for large tip-sample separations, the relatively sudden onset of short-range repulsive forces due to overlapping electron clouds introduces strong nonlinearities in the system description [6,7]. Similarly, in the (common) presence of thin films of water covering the sample and the probe tip due to the humidity in the surrounding air (e.g., Refs. [8–10]), the relatively sudden onset and cessation of capillary force interactions introduce apparent jumps in the force field with the additional feature that cessation occurs for separations larger than those at onset corresponding to hysteresis in the force description [11].

In conjunction with the nonlinearities present in the force interactions in between the events described above, these rapid changes in the nature and magnitude of the interaction forces during intermittent-contact-mode operation result in dramatic transitions in system response [12,13], the possibility of multiple coexisting periodic steady-state responses [14], as well as ranges with high-periodic, quasiperiodic, or irregular system responses [15]. As the predictability of the cantilever response is the foundation for imaging methods using atomic-force microscopy, these nonlinearities must be understood, compensated for if necessary, or exploited to the advantage of imaging if possible [16].

The quantitative study presented in Sec. 3 is motivated by an effort to investigate the essential contribution to the complexity of the system response that originates in the hysteretic force description associated with capillary force interactions. In particular, we emphasize the transitions in system response that occur as the point of closest approach to the sample of a periodic cantilever oscillation occurs in the immediate vicinity of the separation corresponding to the onset of capillary interactions. This follows the approach taken by the present authors and their collaborators in a series of investigations of the transitions in system response that occur as the point of closest approach to the sample of a periodic cantilever oscillation occurs in the immediate vicinity of the separation corresponding to the onset of (nonhysteretic) repulsive forces (e.g., Refs. [17–19]).

As of the present time, only limited effort has been made to

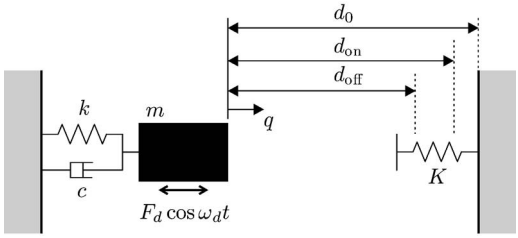


**Fig. 1 A schematic of an example oscillator. Two distinct regimes of interaction between the mass and its environment are represented by the additional spring with stiffness $K$ and zero load when $q=d_0$. Here, $d_{\text{on}}$ denotes the displacement of the mass at which the spring is initially engaged and $d_{\text{off}}$ denotes the displacement of the mass at which the spring is disengaged.**

investigate the influence of the capillary force interactions on the cantilever response. Zitzler et al. [11] explored the influence from capillary force interactions on the transitions between the *attractive* (noncontacting) and *repulsive* (contacting) branches of stable periodic oscillations (cf. Refs. [20–22]). To this end, they assumed that as the instantaneous tip-sample separation $d$ falls below a critical distance $d_{\text{on}}=2h$, where $h$ is the film thickness, a connective column of liquid is established. Upon retracting away from the surface the liquid column forms a meniscus and neck until eventually breaking as the separation increases beyond a critical distance $d_{\text{off}}>d_{\text{on}}$. In the presence of the liquid column, Zitzler et al. [11] modeled the resultant force interaction by the expression

$$\frac{4\pi\gamma_{\text{H}_2\text{O}}R}{1+d/h} \tag{1}$$

where $R$ is the radius of curvature of the cantilever tip, and $\gamma_{\text{H}_2\text{O}}$ is the surface energy of water. In particular, it follows from this expression that both the onset and cessation of the capillary force interactions are associated with discontinuous jumps in the force magnitude.

Where Zitzler et al. [11] chose to numerically smooth the events associated with the onset and cessation of the capillary force interactions for purposes of computer simulation, we contend that the piecewise nature of the system definition should be embraced and exploited in as far as possible so as to reduce the resultant complexity in the system response to its dynamic essence. Indeed, even with a smooth model, it is clear that the rapid (albeit not discontinuous) change in the force description will have a demonstrably large influence on the system response. By purposefully coarsening the vector field to form a piecewise smooth model, a singular event can be identified into which all the complexity resulting from the rapid change is collapsed. A methodology based on this approach should thus capture the gross transition in system response associated with rapid changes in the force description but obviate the need to resolve individual bifurcations.

## 3 An Example Oscillator

**3.1 Model Development.** To isolate the effects associated with a hysteretic discontinuity, consider the example oscillator shown schematically in Fig. 1. Here, the mass $m$ moves under the influence of a linear spring with stiffness $k$, a viscous damper with damping coefficient $c$, and an additional interaction force $F_{\text{int}}$ between the mass and its environment that depends on the instantaneous displacement $q$ of the mass relative to the undeformed length of the spring as well as on the recent displacement history of the mass. Excitation of the oscillator is achieved through the imposition of a sinusoidally varying force with amplitude $F_d$ and angular frequency $\omega_d$.

As suggested in Fig. 1, two distinct regimes of interaction between the mass and its environment will be considered corresponding to the absence or presence of an elastic force resulting from the deformations of an additional spring with stiffness $K$ with zero load when $q=d_0$ for some positive constant $d_0$. Let $d_{\text{on}}>0$ denote the displacement of the mass at which the spring is initially engaged and let $d_{\text{off}}>0$ denote the displacement of the mass at which the spring is disengaged, such that $d_{\text{off}}<d_{\text{on}}$. Then, provided that $d_0 \geq d_{\text{on}}$, it follows that the spring, when engaged, results in an overall softening response.

**Table 1 Each entry in the table represents the transition trigger function for which a zero-crossing from positive to negative values results in a discrete change in the mode variable from its value $\mathfrak{m}_b$ before the triggered event to its value $\mathfrak{m}_a$ after the triggered event**

| | $\mathfrak{m}_a$ | |
|---|---|---|
| $\mathfrak{m}_b$ | Off | On |
| Off | * | $d_{\text{on}}-x_1$ |
| On | $x_1-d_{\text{off}}$ | * |

The dynamics of the oscillator may be described through the introduction of a state vector

$$\mathbf{x}=\begin{pmatrix} x_1 \\ x_2 \\ x_3 \end{pmatrix} \overset{\text{def}}{=} \begin{pmatrix} q \\ \dot{q} \\ \omega_d t \bmod 2\pi \end{pmatrix} \tag{2}$$

and a mode variable $\mathfrak{m}$, such that

$$\frac{d\mathbf{x}}{dt}=\mathbf{f}_{\mathfrak{m}}(\mathbf{x}) \overset{\text{def}}{=} \begin{pmatrix} x_2 \\ \dfrac{1}{m}(F_d \cos x_3 - cx_2 - kx_1 + F_{\text{int}}(x_1,\mathfrak{m})) \\ \omega_d \end{pmatrix} \tag{3}$$

where

$$F_{\text{int}}(q,\mathfrak{m})=\begin{cases} 0 & \text{when } \mathfrak{m}=\text{off} \\ K(d_0-q) & \text{when } \mathfrak{m}=\text{on} \end{cases} \tag{4}$$

and $x_3$ corresponds to the instantaneous *phase* of the excitation.

Table 1 shows the discrete changes in the value of the index variable that occur as a result of zero-crossings of certain *transition trigger functions* (event functions) from positive to negative values. In particular, let $h_{\text{on}}(\mathbf{x})=d_{\text{on}}-x_1$ and $h_{\text{off}}(\mathbf{x})=x_1-d_{\text{off}}$. Then, a mode transition from $\mathfrak{m}=$off to $\mathfrak{m}=$on occurs at a time $t^*$ provided that $h_{\text{on}}(\mathbf{x}(t^*))=0$ and $h_{\text{on}}(\mathbf{x}(t))$ is a decreasing function of $t$ on an interval containing $t^*$. Similarly, a mode transition from $\mathfrak{m}=$on to $\mathfrak{m}=$off occurs at a time $t^*$ provided that $h_{\text{off}}(\mathbf{x}(t^*))=0$ and $h_{\text{off}}(\mathbf{x}(t))$ is a decreasing function of $t$ on an interval containing $t^*$. In particular, it follows that for trajectory segments governed by $\mathbf{f}_{\text{off}}$ that enter the interval $d_{\text{off}}<x_1<d_{\text{on}}$, the value $\mathfrak{m}=$off of the mode variable is retained until such a time that the value of $x_1$ exceeds $d_{\text{on}}$. Similarly, for trajectory segments governed by $\mathbf{f}_{\text{on}}$ that enter this interval, the value $\mathfrak{m}=$on of the mode variable is retained until such a time that the value of $x_1$ falls below $d_{\text{off}}$. A consistent value of the mode variable for states in this interval thus depends on the past displacement history of the mass and not simply on its current value as would be the case in the absence of hysteresis.

For initial conditions on the zero-level surfaces of the transition trigger functions, past displacement history does not necessarily suffice to determine the appropriate subsequent value for the mode variable. No ambiguity exists in cases where the time evolution of the sign of the corresponding transition trigger function is the same along trajectory segments of either vector field based at such an initial condition. For example, for initial conditions on $h_{\text{on}}=0$ for which

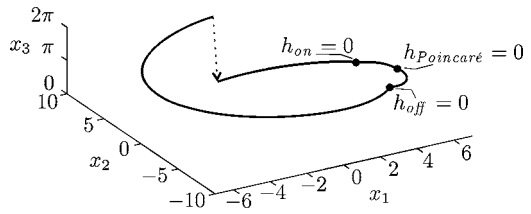


**Fig. 2 A sample periodic trajectory of the example oscillator with $F_d \approx 6.93$. Here, dots refer to zero-crossings of the event functions corresponding to the onset and cessation of interactions with the additional linear spring and the Poincaré sampling trigger function. The dashed line refers to the instantaneous change in $x_3$ from $2\pi$ to 0 that results from its definition.**

$$\left.\frac{d}{dt}h_{\text{on}}(\mathbf{x}(t))\right|_{t=0,\ \dot{\mathbf{x}}=\mathbf{f}_{\text{off}}} \cdot \left.\frac{d}{dt}h_{\text{on}}(\mathbf{x}(t))\right|_{t=0,\ \dot{\mathbf{x}}=\mathbf{f}_{\text{on}}} > 0 \tag{5}$$

the appropriate value of the mode variable equals $\mathfrak{m}=$on if

$$\left.\frac{d}{dt}h_{\text{on}}(\mathbf{x}(t))\right|_{t=0,\ \dot{\mathbf{x}}=\mathbf{f}_{\text{on}}} < 0 \tag{6}$$

and $\mathfrak{m}=$off otherwise. Since here

$$\left.\frac{d}{dt}h_{\text{on}}(\mathbf{x}(t))\right|_{t=0,\ \dot{\mathbf{x}}=\mathbf{f}_{\text{on}}} = \left.\frac{d}{dt}h_{\text{on}}(\mathbf{x}(t))\right|_{t=0,\ \dot{\mathbf{x}}=\mathbf{f}_{\text{on}}} = -x_2 \tag{7}$$

such *transversal* crossings occur provided that a zero-crossing of $h_{\text{on}}$ from positive to negative values is reached with nonzero velocity. In contrast, degenerate situations corresponding to *grazing contact*, for which

$$\left.\frac{d}{dt}h_{\text{on}}(\mathbf{x}(t))\right|_{t=0,\ \dot{\mathbf{x}}=\mathbf{f}_{\text{off}}} \cdot \left.\frac{d}{dt}h_{\text{on}}(\mathbf{x}(t))\right|_{t=0,\ \dot{\mathbf{x}}=\mathbf{f}_{\text{on}}} = 0 \tag{8}$$

must be handled on a case-by-case basis.

For $d_0$ distinct from $d_{\text{on}}$, the variations in the interaction force are discontinuous across transitions between $\mathfrak{m}=$off and $\mathfrak{m}=$on and vice versa. In contrast, if $d_0$ agrees with $d_{\text{on}}$ the interaction force equals 0 as the spring is first engaged, resulting in a continuous transition of the interaction force between $\mathfrak{m}=$off and $\mathfrak{m}=$on.

Now consider the *sampling trigger function* $h_{\text{Poincaré}}(\mathbf{x})=x_2$, such that the sampling occurs at a time $t^*$ provided that $h_{\text{Poincaré}}(\mathbf{x}(t^*))=0$ and $h_{\text{Poincaré}}(\mathbf{x}(t))$ is a decreasing function of $t$ on some interval containing $t^*$. In particular, transversal crossings of the zero-level surface $h_{\text{Poincaré}}=0$ correspond to a record of the sampled values of the state vector at moments when the excursion of the mass achieves a local maximum. In the case of a periodic response of the oscillator with period equal to that of the excitation, the sampled value of $\omega_d t \bmod 2\pi$ equals the *phase lag* of the response relative to the excitation (which achieves its maximum value at $\omega_d t \bmod 2\pi=0$).

As an example of the results of the forward-time simulation and Poincaré sampling, Fig. 2 shows a finite solution segment of the example oscillator with parameter values given in Table 2. Here, the forward-time simulation was implemented using MATLAB's ode integrators and the corresponding event-handling functionality.

**Table 2 Values of the system parameters in a consistent set of units used in the numerical analysis of the example oscillator**

| | | |
|---|---|---|
| Mass | $m$ | 1 |
| Stiffness | $k$ | 1 |
| Damping coefficient | $c$ | 1 |
| Interaction stiffness | $K$ | 3 |
| Zero-load distance | $d_0$ | 7 |
| Onset of capillary forces | $d_{\text{on}}$ | 6 |
| Cessation of capillary forces | $d_{\text{off}}$ | 5 |
| Excitation frequency | $\omega_d$ | 1 |

**3.2 Linearized Dynamics.** Let $\mathbf{\Phi}_{\text{on}}$ and $\mathbf{\Phi}_{\text{off}}$ denote the *flow functions* corresponding to the vector fields $\mathbf{f}_{\text{on}}$ and $\mathbf{f}_{\text{off}}$, i.e., such that

$$\frac{d}{dt}\mathbf{\Phi}_{\mathfrak{m}}(\mathbf{x},t) = \mathbf{f}_{\mathfrak{m}}(\mathbf{\Phi}_{\mathfrak{m}}(\mathbf{x},t)) \tag{9}$$

and $\mathbf{\Phi}_{\mathfrak{m}}(\mathbf{x},0)=\mathbf{x}$, where $\mathbf{x}$ is the initial state and $\mathfrak{m}=$on or off. For trajectory segments governed by the $\mathbf{f}_{\mathfrak{m}}$ vector field and terminating away from a mode transition, the matrix of first partial derivatives of the components of the flow with respect to the components of the initial state $\partial_{\mathbf{x}}\mathbf{\Phi}_{\mathfrak{m}}(\mathbf{x},t)$ describes the sensitivity of the final state after elapsed time $t$ to perturbations in the initial state. In particular, by differentiation of the defining relationships for the flow function, it follows that

$$\frac{d}{dt}\partial_{\mathbf{x}}\mathbf{\Phi}_{\mathfrak{m}}(\mathbf{x},t) = \partial_{\mathbf{x}}\mathbf{f}_{\mathfrak{m}}(\mathbf{\Phi}_{\mathfrak{m}}(\mathbf{x},t)) \cdot \partial_{\mathbf{x}}\mathbf{\Phi}_{\mathfrak{m}}(\mathbf{x},t) \tag{10}$$

and $\partial_{\mathbf{x}}\mathbf{\Phi}_{\mathfrak{m}}(\mathbf{x},0)=\text{Id}$, where Id is the identity matrix.

Consider, instead, a trajectory segment governed by the vector field $\mathbf{f}_{\mathfrak{m}}$, based at an initial condition $\mathbf{x}_0$, and terminating after an elapsed time $\tau$ at a transversal crossing $\mathbf{x}_1$ with the zero-level surface of some transition trigger function $h_{\mathfrak{e}}$. Then, by the transversality of the crossing, there exists a map $\mathbf{\Pi}$ that maps nearby initial conditions $\mathbf{x}\approx\mathbf{x}_0$ to the corresponding unique transversal crossings of $h_{\mathfrak{e}}=0$ at points $\mathbf{\Pi}(\mathbf{x})\approx\mathbf{x}_1$ after elapsed times close to $\tau$, such that

$$\partial_{\mathbf{x}}\mathbf{\Pi}(\mathbf{x}_0) = \left(\text{Id} - \frac{\mathbf{f}_{\mathfrak{m}}(\mathbf{x}_1)\cdot\partial_{\mathbf{x}}h_{\mathfrak{e}}(\mathbf{x}_1)}{\partial_{\mathbf{x}}h_{\mathfrak{e}}(\mathbf{x}_1)\cdot\mathbf{f}_{\mathfrak{m}}(\mathbf{x}_1)}\right)\cdot\partial_{\mathbf{x}}\Phi_{\mathfrak{m}}(\mathbf{x}_0,\tau) \tag{11}$$

describes the sensitivity of the point of transversal crossing to perturbations in the initial state [3].

Now consider a periodic trajectory consisting of a finite sequence $\xi=\{\mathbf{x}_j(t), t_{j-1}\le t\le t_j\}_{j=1}^N$ of trajectory segments and an associated sequence $\{\mathfrak{m}_j\}_{j=1}^N$ of values of the mode variable, where $\mathbf{x}_N(t_N)=\mathbf{x}_1(t_0)$ and such that each trajectory segment terminates at a transversal crossing with the zero-level surface of some transition trigger function. Then, by composition of the maps $\mathbf{\Pi}$ introduced previously, a global Poincaré mapping $\mathbf{P}$ may be defined from any one of the zero-level surfaces and back to the same zero-level surface on some neighborhood of the intersection of the periodic trajectory with this zero-level surface. In particular, the sensitivity of $\mathbf{P}(\mathbf{x})$ to perturbations in the initial state is given by a product of matrices of the form (11).

As long as (i) all terminal points of the segments on a periodic trajectory are transversal crossings, (ii) no points of grazing contact with the zero-level surface of some transition trigger function occur along any segment, and (iii) the sensitivity matrix of the composite Poincaré mapping $\mathbf{P}$ has no eigenvalues on the unit circle, the implicit function theorem guarantees the continuous persistence of the periodic trajectory under variations in system parameters. It follows that path continuation can be employed to trace branches of periodic trajectories under selected variations of system parameters.

**3.3 System Response.** The smooth dynamical system governed entirely by the $\mathbf{f}_{\text{off}}$ vector field has a unique family of steady-state periodic attractors given by

$$q(t) = A_0\cos(\omega_d t - \theta) \tag{12}$$

where

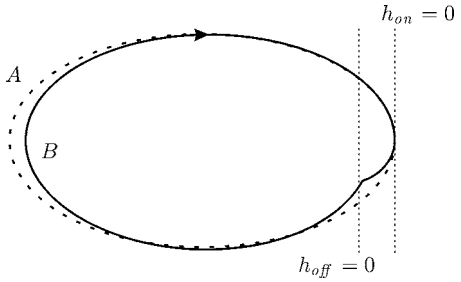


**Fig. 3 Periodic solutions that achieve grazing contact with $h_{on}=0$ in state space. Here, the dashed trajectory is governed entirely by the $f_{off}$ vector field, whereas the solid trajectory includes a segment governed by $f_{on}$.**

$$A_0 = \frac{F_d}{\sqrt{(k - m\omega_d^2)^2 + (c\omega_d)^2}} \tag{13}$$

is the amplitude of oscillation and the phase lag $\theta$ satisfies the equation

$$\tan\theta = \frac{c\omega_d}{k - m\omega_d^2} \tag{14}$$

In the case of the example oscillator with the hysteretic interaction force, these attractors persist with a finite basin of attraction as long as $A_0 < d_{\text{on}}$. On the other hand, for $d_{\text{on}} < A_0$ no steady-state attractor exists for which $\mathfrak{m}$ remains equal to off throughout.

The branch of periodic trajectories governed entirely by the $\mathbf{f}_{\text{off}}$ vector field can be uniquely characterized by the corresponding points of transversal intersection

$$\mathbf{x}^*(A_0) = \begin{pmatrix} A_0 \\ 0 \\ \theta \end{pmatrix} \tag{15}$$

with the zero-level surface of the $h_{\text{Poincaré}}$ sampling trigger function. Following the discussion in Sec. 3.2, it follows that, for each value of $A_0 \leq d_{\text{on}}$, $\mathbf{x}^*(A_0)$ is a unique fixed point of the associated Poincaré mapping $\mathbf{P}$ defined entirely from the $\mathbf{f}_{\text{off}}$ vector field. In particular, the terminal point on this branch of periodic trajectories under variations in $A_0$ corresponds to a fixed point $\mathbf{x}^*(d_{\text{on}})$ of $\mathbf{P}$ that is a point of grazing contact with the $h_{\text{on}}=0$ surface (cf. dashed trajectory in Fig. 3). Indeed, since

$$\frac{d^2}{dt^2} h_{\text{on}}(\mathbf{x}(t))\Big|_{\substack{\mathbf{x}(t)=\mathbf{x}^*(d_{\text{on}}) \\ \dot{\mathbf{x}}=\mathbf{f}_{\text{off}}}} = \omega_d^2 d_{\text{on}} > 0 \tag{16}$$

$\mathbf{x}^*(d_{\text{on}})$ is a simple local minimum of $h_{\text{on}}$ along trajectories governed by $\mathbf{f}_{\text{off}}$. By continuity, it follows that nearby trajectories governed by $\mathbf{f}_{\text{off}}$ also have simple local minima in the value of $h_{\text{on}}$ on $h_{\text{Poincaré}}=0$, some of which occur at points with $h_{\text{on}}<0$.

For the terminal point, the linearized description of the local behavior of nearby trajectories given by $\partial_{\mathbf{x}}\mathbf{P}(\mathbf{x}^*(d_{\text{on}}))$ fails to account for the mode transition associated with a crossing of the $h_{\text{on}}=0$ surface that applies to a subset of nearby trajectories and that results in the onset of a finite perturbation to the applied force. This perturbation persists until a subsequent transition to $\mathfrak{m}$=off that occurs, if at all, only after a finite elapsed time that remains bounded from below as the initial condition approaches $\mathbf{x}^*(d_{\text{on}})$. The simple grazing point $\mathbf{x}^*(d_{\text{on}})$ thus lies on a boundary across which solutions are discontinuous with respect to initial conditions. It follows that the periodic trajectory corresponding to $\mathbf{x}^*(d_{\text{on}})$ is unstable to perturbations in the initial state. Moreover, no branch of periodic trajectories that intersect $h_{\text{Poincaré}}=0$ at points with $h_{\text{on}}<0$ can emanate continuously from the grazing

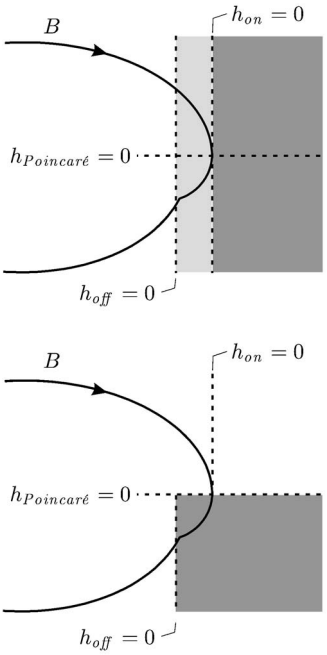


**Fig. 4 The solid trajectory in Fig. 3 is a solution to the original hybrid dynamical system with hysteresis shown in the upper panel as well as the alternative piecewise smooth dynamical system without hysteresis shown in the lower panel**

periodic trajectory.

Periodic trajectories that involve switching between $\mathfrak{m}$=on and $\mathfrak{m}$=off are not directly amenable to closed-form analysis. Special limiting cases of such trajectories, in which one trajectory segment switches from $\mathfrak{m}$=off to $\mathfrak{m}$=on at a point of grazing contact with $h_{\text{on}}=0$, can nevertheless be investigated with perturbation techniques particular to the study of hybrid dynamical systems.

To illustrate the methodology, consider an alternative dynamical system governed by the same vector fields, but for which $\mathfrak{m}$=off provided that $h_{\text{off}}<0$ or $h_{\text{Poincaré}}>0$ and $\mathfrak{m}$=on provided that $h_{\text{off}}>0$ and $h_{\text{Poincaré}}<0$ (cf. Fig. 4). Suppose that, for some critical value of some system parameter $\mu=\mu^*$, there exists a periodic trajectory of this system consisting of a trajectory segment based on the point $\mathbf{x}^*(\mu^*)$ on $h_{\text{Poincaré}}=0$ and governed by $\mathbf{f}_{\text{on}}$ that terminates at a transversal mode transition on $h_{\text{off}}=0$ followed by a trajectory segment governed by $\mathbf{f}_{\text{off}}$ and terminating at $\mathbf{x}^*(\mu^*)$ at a transversal mode transition on $h_{\text{Poincaré}}=0$. By the previous analysis, it is possible to define a Poincaré mapping $\tilde{\mathbf{P}}$ corresponding to this alternative dynamical system, such that the intersection of the periodic trajectory with $h_{\text{Poincaré}}=0$ is a fixed point of $\tilde{\mathbf{P}}$. Assuming hyperbolicity (i.e., no eigenvalues on the unit circle), persistence of a branch of periodic trajectories of this alternative dynamical system under variations in the value of the system parameter $\mu$ again follows from the implicit function theorem.

Nearby trajectories of the alternative dynamical system are not generally solutions to the original oscillator dynamics. For intersections with $h_{\text{Poincaré}}=0$ that occur at points with $h_{\text{on}}>0$, the switch to $\mathbf{f}_{\text{on}}$ is not a mode transition of the original system. Similarly, for intersections with $h_{\text{Poincaré}}=0$ that occur at points with $h_{\text{on}}<0$, the mode transition to $\mathfrak{m}$=on that should have accompanied a previous crossing of $h_{\text{on}}=0$ has not been correctly accounted for.

To accommodate the distinction between the two dynamical systems, consider the special case, for which the fixed point

$$\mathbf{x}^*(\mu^*) = \begin{pmatrix} d_{\text{on}} \\ 0 \\ \theta^* \end{pmatrix} \tag{17}$$

of $\tilde{\mathbf{P}}$ lies on $h_{\text{on}}=0$ and is a simple local minimum in the value of $h_{\text{on}}$ along trajectory segments governed by either vector field, i.e., such that

$$a_1 \overset{\text{def}}{=} \left.\frac{d^2}{dt^2} h_{\text{on}}(\mathbf{x}(t))\right|_{\mathbf{x}(t)=\mathbf{x}^*(\mu^*),\ \dot{\mathbf{x}}=\mathbf{f}_{\text{off}}} > 0 \tag{18}$$

and

$$a_2 \overset{\text{def}}{=} \left.\frac{d^2}{dt^2} h_{\text{on}}(\mathbf{x}(t))\right|_{\mathbf{x}(t)=\mathbf{x}^*(\mu^*),\ \dot{\mathbf{x}}=\mathbf{f}_{\text{on}}} = a_1 - \frac{K}{m}(d_0 - d_{\text{on}}) > 0 \tag{19}$$

By continuity, it again follows that nearby trajectories governed by either vector field also have simple local minima in the value of $h_{\text{on}}$ on $h_{\text{Poincaré}}=0$. From the Taylor expansion

$$\mathbf{\Phi}_{\mathfrak{m}}(\mathbf{x},t) = \mathbf{x} + t\mathbf{f}_{\mathfrak{m}}(\mathbf{x}) + \frac{t^2}{2}\partial_{\mathbf{x}}\mathbf{f}_{\mathfrak{m}}(\mathbf{x}) \cdot \mathbf{f}_{\mathfrak{m}}(\mathbf{x}) + \mathcal{O}(t^3) \tag{20}$$

it follows that, for trajectories governed by $\mathbf{f}_{\text{off}}$ and based at such a simple minimum

$$\mathbf{x}_0 = \begin{pmatrix} d_{\text{on}} + \varepsilon^2 \\ 0 \\ \theta^* + \varepsilon\Delta\theta \end{pmatrix} \tag{21}$$

with $h_{\text{on}}(\mathbf{x}_0) = -\varepsilon^2 < 0$ for some $0 < \varepsilon \ll 1$,

$$h_{\text{on}}(\mathbf{\Phi}_{\text{off}}(\mathbf{x}_0,t)) = -\varepsilon^2 + a_1\frac{t^2}{2} + \mathcal{O}(t^3, \varepsilon t^2) \tag{22}$$

The elapsed time since the previous intersection with $h_{\text{on}}=0$ is then given by

$$\varepsilon\sqrt{\frac{2}{a_1}} + \mathcal{O}(\varepsilon^2) \tag{23}$$

and the corresponding point of intersection is given by

$$\mathbf{x}_1 = \begin{pmatrix} d_{\text{on}} \\ \varepsilon\sqrt{\dfrac{2}{a_1}}a_1 + \mathcal{O}(\varepsilon^2) \\ \theta^* + \varepsilon\left(\Delta\theta - \omega_d\sqrt{\dfrac{2}{a_1}}\right) + \mathcal{O}(\varepsilon^2) \end{pmatrix} \tag{24}$$

For the trajectory segment governed by $\mathbf{f}_{\text{on}}$ and based at $\mathbf{x}_1$,

$$h_{\text{Poincaré}}(\mathbf{\Phi}_{\text{on}}(\mathbf{x}_1,t)) = \varepsilon\sqrt{\frac{2}{a_1}}a_1 - ta_2 + \mathcal{O}(\varepsilon^2, \varepsilon t, t^2) \tag{25}$$

The elapsed time until the subsequent intersection with $h_{\text{Poincaré}}=0$ is then given by

$$\varepsilon\sqrt{\frac{2}{a_1}}\frac{a_1}{a_2} + \mathcal{O}(\varepsilon^2) \tag{26}$$

and the corresponding point of intersection is given by

$$\mathbf{x}_2 = \begin{pmatrix} d_{\text{on}} + \mathcal{O}(\varepsilon^2) \\ 0 \\ \theta^* + \varepsilon\left(\Delta\theta - \omega_d\sqrt{\dfrac{2}{a_1}}\left(1 - \dfrac{a_1}{a_2}\right)\right) + \mathcal{O}(\varepsilon^2) \end{pmatrix} \tag{27}$$

In particular, $\mathbf{x}_2$ is the point on $h_{\text{Poincaré}}=0$ that would have been reached by the flow of the original dynamical system had the mode transition to $\mathfrak{m}=\text{on}$ been correctly imposed.

The *discontinuity-mapping* $\mathbf{D}:\mathbf{x}_0 \mapsto \mathbf{x}_2$ thus accounts for the correction to the Poincaré mapping $\tilde{\mathbf{P}}$ that must be imposed for trajectories that intersect $h_{\text{Poincaré}}=0$ near $\mathbf{x}^*(\mu^*)$ with $h_{\text{on}}<0$ (see Fig. 5). Indeed, iterates of the composition $\tilde{\mathbf{P}}\circ\mathbf{D}$ respect the dynamics of the original system as long as all sampled points occur with $h_{\text{on}}<0$. In particular, fixed points of $\tilde{\mathbf{P}}\circ\mathbf{D}$ on $h_{\text{Poincaré}}=0$ with $h_{\text{on}}<0$ correspond to periodic trajectories of the original oscillator dynamics.

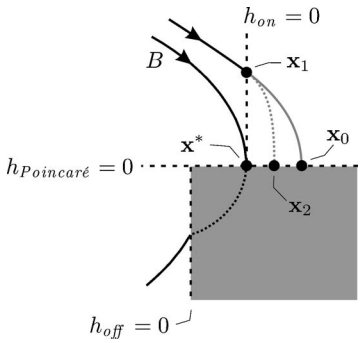


**Fig. 5 The discontinuity-mapping $\mathbf{D}:\mathbf{x}_0 \mapsto \mathbf{x}_2$ accounts for the correction to the local flow. Here, solid curves correspond to the $\Phi_{\text{off}}$ flow and dashed curves correspond to the $\Phi_{\text{on}}$ flow.**

Provided that $h_{\text{on}}$ is independent of $\mu$, it is straightforward to show that, to the expressed order in $\varepsilon$, the expression for $\mathbf{D}$ is valid for $\Delta\mu \overset{\text{def}}{=} \mu - \mu^* = \mathcal{O}(\varepsilon)$. Now suppose that

$$\partial_{\mathbf{x}}\tilde{\mathbf{P}}(\mathbf{x}^*(\mu^*),\mu^*) = \begin{pmatrix} P_{11} & P_{12} & P_{13} \\ 0 & 0 & 0 \\ P_{31} & P_{32} & P_{33} \end{pmatrix} \tag{28}$$

and

$$\partial_{\mu}\tilde{\mathbf{P}}(\mathbf{x}^*(\mu^*),\mu^*) = \begin{pmatrix} P_{1\mu} \\ 0 \\ P_{3\mu} \end{pmatrix} \tag{29}$$

Then, to order $\mathcal{O}(\varepsilon^2)$, the composition $\tilde{\mathbf{P}}\circ\mathbf{D}$ reduces to the map

$$\begin{pmatrix} q \\ \theta \end{pmatrix} \mapsto \begin{pmatrix} d_{\text{on}} + P_{13}(\theta_2 - \theta^*) + P_{1\mu}\Delta\mu \\ \theta^* + P_{33}(\theta_2 - \theta^*) + P_{3\mu}\Delta\mu \end{pmatrix} \tag{30}$$

where

$$\theta_2 = \theta - \omega_d\sqrt{\frac{2}{a_1}}\left(1 - \frac{a_1}{a_2}\right)\sqrt{q - d_{\text{on}}} \tag{31}$$

A family of fixed points $\mathbf{x}^*(\mu)$ of $\tilde{\mathbf{P}}\circ\mathbf{D}$ is given by

$$\theta^*(\mu) = \theta^*(\mu^*) + \frac{P_{3\mu}P_{13} - P_{1\mu}P_{33}}{P_{13}}\Delta\mu \tag{32}$$

$$\sqrt{q^*(\mu) - d_{\text{on}}} = \frac{P_{1\mu}(1 - P_{33}) + P_{13}P_{3\mu}}{P_{13}\omega_d\sqrt{\dfrac{2}{a_1}}\left(1 - \dfrac{a_1}{a_2}\right)}\Delta\mu \tag{33}$$

i.e., such that the value of $h_{\text{on}}$ along this family goes as the square of the deviation in the system parameter. In particular, the corresponding branch of periodic trajectories emanates from $\mathbf{x}^*(\mu^*)$ in the direction of increasing values of $\mu$ provided that

$$\frac{P_{1\mu}(1 - P_{33}) + P_{13}P_{3\mu}}{P_{13}} < 0 \tag{34}$$

and in the direction of decreasing values of $\mu$ provided that

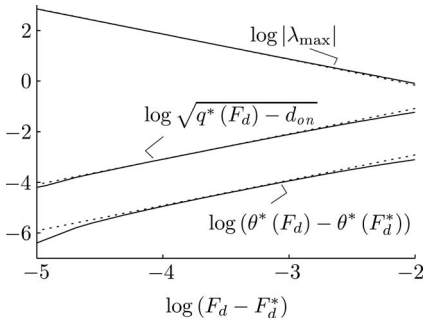


**Fig. 6 Branch of periodic trajectories emanating from the solid trajectory in Fig. 3 characterized by the corresponding values of $\sqrt{q-d_{on}}$ and $\theta$ at the intersection with $h_{Poincaré}=0$ (when ignoring the mode transition associated with a crossing with $h_{on}=0$) as well as the largest-in-magnitude eigenvalue. Here, the dashed curves are the predictions from the discontinuity-mapping analysis, whereas the solid curves are obtained from the numerical continuation.**

$$\frac{P_{1\mu}(1-P_{33})+P_{13}P_{3\mu}}{P_{13}}>0 \tag{35}$$

Finally, the eigenvalues of $\partial_{\mathbf{x}}(\tilde{\mathbf{P}}\circ\mathbf{D})$ about this fixed point are

$$0, P_{33}-\left(1-\frac{a_1}{a_2}\right)\frac{P_{13}\omega_d}{\sqrt{q^*(\mu)-d_{\text{on}}}}\sqrt{\frac{1}{2a_1}} \tag{36}$$

As $\mu\to\mu^*$ and, consequently, $q^*(\mu)\to d_{\text{on}}$, one of these goes to $\infty$ if $P_{13}>0$ and to $-\infty$ if $P_{13}<0$.

For $F_d^*\approx 6.19685$ there exists a periodic trajectory governed by the alternative hybrid dynamical system that intersects $h_{\text{Poincaré}}=0$ at a point where $h_{\text{on}}=0$ and $x_3^*\approx 1.59454$ (see solid trajectory in Fig. 3). For this trajectory, $P_{13}\approx -0.218099$, $P_{33}\approx 0.0288904$, $P_{1F_d}\approx 0.998439$, and $P_{3F_d}\approx -0.0105249$. Since, in this case

$$\frac{P_{1F_d}(1-P_{33})+P_{13}P_{3F_d}}{P_{13}}\approx -4.45619<0 \tag{37}$$

it follows that a branch of periodic trajectories of the original dynamical system emanates from this periodic trajectory as $F_d$ increases from $F_d^*$. Moreover, since $P_{13}<0$ one of the eigenvalues goes to $-\infty$ as the $F_d$ approaches $F_d^*$ from above. These claims are confirmed by the numerical results reported in Fig. 6. In particular, for deviations $F_d-F_d^*$ from $10^{-5}$ to $10^{-2}$ the predicted linear dependence of $\sqrt{q^*(F_d)-d_{\text{on}}}$ and $\theta^*(F_d)$ on this deviation as well as the corresponding linear coefficient are in close agreement with results obtained through numerical continuation. This is also the case for the magnitude of the largest-in-magnitude eigenvalue, which appears inversely proportional to the deviation $F_d-F_d^*$ as predicted by the discontinuity-mapping analysis.

## 4 Conclusions

As demonstrated here, the discontinuity-mapping technique provides an unfolding of the local behavior of a hybrid dynamical system in the vicinity of certain discontinuity-induced singularities, in this case the grazing contact with a surface representing the onset of a hysteretic force interaction. The application of this methodology to the model of the capillary force interactions proposed by Zitzler et al. [11] will be the objective of future work. This should also include an effort to investigate further the system response immediately past a branch termination point and to seek to establish the extent to which this might also be amenable to the discontinuity-mapping analysis.

## Acknowledgment

This material is based on the work supported by the National Science Foundation under Grant Nos. 0510044 and 0619028, a GOALI project performed in collaboration with Veeco Metrology, LLC.

## References

[1] di Bernardo, M., Budd, C. J., and Champneys, A. R., 2001, "Normal Form Maps for Grazing Bifurcations in *n*-Dimensional Piecewise-Smooth Dynamical Systems," Physica D, **160**(3–4), pp. 222–254.
[2] Nordmark, A. B., 1997, "Universal Limit Mapping in Grazing Bifurcations," Phys. Rev. E, **55**(1), pp. 266–270.
[3] di Bernardo, M., Budd, C. J., Champneys, A. R., and Kowalczyk, P., 2008, *Piecewise-Smooth Dynamical Systems: Theory and Applications*, Springer-Verlag, New York.
[4] Fredriksson, M. H., and Nordmark, A. B., 1961, "Bifurcations Caused by Grazing Incidence in Many Degrees of Freedom Impact Oscillators," Proc. R. Soc. London, Ser. A, **453**, pp. 1261–1276.
[5] Dankowicz, H., and Nordmark, A. B., 2000, "On the Origin and Bifurcations of Stick-Slip Oscillations," Physica D, **136**(3–4), pp. 280–302.
[6] Lee, S. I., Howell, S. W., Raman, A., and Reifenberger, R., 2002, "Nonlinear Dynamics of Microcantilevers in Tapping Mode Atomic Force Microscopy: A Comparison Between Theory and Experiment," Phys. Rev. B, **66**(11), p. 115409.
[7] Lee, S. I., Howell, S. W., Raman, A., and Reifenberger, R., 2003, "Nonlinear Dynamic Perspectives on Dynamic Force Microscopy," Ultramicroscopy, **97**(1–4), pp. 185–198.
[8] Beaglehole, D., and Christenson, H. K., 1992, "Vapor Adsorption on Mica and Silicon: Entropy Effects, Layering, and Surface Forces," J. Phys. Chem., **96**(8), pp. 3395–3403.
[9] Jang, J., Schatz, G. C., and Ratner, M. A., 2004, "Capillary Force in Atomic Force Microscopy," J. Chem. Phys., **120**(3), pp. 1157–1160.
[10] Garcia-Martin, A., and Garcia, R., 2006, "Formation of Nanoscale Liquid Menisci in Electric Fields," Appl. Phys. Lett., **88**(12), p. 123115.
[11] Zitzler, L., Herminghaus, S., and Mugele, F., 2002, "Capillary Force in Tapping Mode Atomic Force Microscopy," Phys. Rev. B, **66**(15), p. 155436.
[12] Garcia, R., and San Paulo, A., 1999, "Attractive and Repulsive Tip-Sample Interaction Regimes in Tapping-Mode Atomic Force Microscopy," Phys. Rev. B, **60**(7), pp. 4961–4967.
[13] Garcia, R., and Perez, R., 2002, "Dynamic atomic force microscopy method," Surf. Sci. Rep., **47**(6–8), pp. 197–301.
[14] Yagasaki, K., 2004, "Nonlinear Dynamics of Vibrating Microcantilevers in Tapping-Mode Atomic Force Microscopy," Phys. Rev. B, **70**(24), p. 245419.
[15] Hashemi, N., Dankowicz, H., and Paul, M. R., 2008, "The Nonlinear Dynamics of Tapping Mode Atomic Force Microscopy With Capillary Force Interaction," J. Appl. Phys., **103**(9), p. 093512.
[16] Dankowicz, H., 2006, "Nonlinear Dynamics as an Essential Tool for Non-Destructive Characterization of Soft Nanostructures Using Tapping-Mode Atomic Force Microscopy," Philos. Trans. R. Soc. London, Ser. A, **364**, pp. 3505–3520.
[17] Misra, S., Dankowicz, H., and Paul, M. R., 2008, "Event-Driven Feedback Tracking and Control of Tapping-Mode Atomic Force Microscopy," Philos. Trans. R. Soc. London, Ser. A, **464**(2096), pp. 2113–2133.
[18] Dankowicz, H., Zhao, X., and Misra, S., 2007, "Near-Grazing Dynamics in Tapping-Mode Atomic Force Microscopy," Int. J. Non-Linear Mech., **42**(4), pp. 697–709.
[19] Zhao, X., and Dankowicz, H., 2006, "Characterization of Intermittent Contact in Tapping Mode Atomic Force Microscopy," ASME J. Comput. Nonlinear Dyn., **1**(2), pp. 109–115.
[20] Thota, P., MacLaren, S., and Dankowicz, H., 2007, "Controlling Bistability in Tapping-Mode AFM Using Dual Frequency Excitation," Appl. Phys. Lett., **91**(9), p. 093108.
[21] Hashemi, N., Paul, M., and Dankowicz, H., 2007, "Exploring the Basins of Attraction of Tapping-Mode Atomic Force Microscopy With Capillary Force Interactions," *Proceedings of the 2007 ASME International Mechanical Engineering Congress and Exposition*, Seattle, WA, Paper No. 062807.
[22] Hashemi, N., Paul, M. R., Dankowicz, H., Lee, M., and Jhe, W., 2008, "The Dissipated Power in Atomic Force Microscopy Due to Interactions With a Capillary Fluid Layer," J. Appl. Phys., **104**(6), p. 063518.